

Ferroelectric Domain Structure of $\text{SrBi}_2\text{Nb}_2\text{O}_9$ Epitaxial Thin Films

M. A. Zurbuchen,* G. Asayama, and D. G. Schlom

Department of Materials Science and Engineering, The Pennsylvania State University, University Park, Pennsylvania 16803-6602

S. K. Streiffer

Materials Science Division, Argonne National Laboratory, Argonne, Illinois 60439

(Received 4 September 2001; published 25 February 2002)

The domain structure in a ferroelectric with well-defined crystallography and negligible ferroelastic distortion ($<0.002\%$) is reported. In contrast to prototypical ferroelectrics in which long-range elastic strain dictates the domain structure, in $\text{SrBi}_2\text{Nb}_2\text{O}_9$ the elastic term is insignificant, allowing dipole-dipole interactions and domain wall energies to dominate in determining the domain structure. Electron microscopy reveals ferroelectric domains that are irregularly shaped and highly curved. Out-of-phase boundary defects are shown to be weakly correlated with 90° ferroelectric domain structure.

DOI: 10.1103/PhysRevLett.88.107601

PACS numbers: 77.80.Dj, 61.72.Nn, 68.37.Lp, 77.84.Dy

The ferroelastic distortions accompanying ferroelectricity range from several percent to vanishingly small. Thus, the contribution of elastic energy to the morphology of ferroelectric domains and to the processes by which they reorient varies by several orders of magnitude for different ferroelectric material systems. Domain wall orientations dictated by spontaneous strain alone are relatively well understood, and can be predicted based on group-theory arguments or using the mechanical compatibility analytical methods of Fousek and Janovec [1]. Indeed a great deal of work on the domain structure of high-ferroelastic-distortion systems has been done [2–5]. In contrast, only very few preliminary studies on crystallographically well-defined ferroelectric systems of low ferroelastic distortion have been performed [6–8], particularly by experimental techniques. Recent simulations [9–12] have addressed some issues concerning the relative magnitudes of long-range elastic strain, domain wall, and electrostatic and dipole-dipole contributions to ferroelectric domain structure [13–15], but a consensus remains to be reached. Little is known about the three-dimensional domain morphologies that form in ferroelectrics with minimal ferroelastic distortion, or about changes in domain reorientation processes relative to high spontaneous strain systems. Of particular interest is switching in constrained geometries, in that it is desired to control all reorientation mechanisms that are active in a ferroelectric thin film. The clamping effect of a constraint has been qualitatively shown to suppress some reorientation mechanisms, e.g., 90° rotation domain switching in high-distortion tetragonal $\text{Pb}(\text{Zr}_x\text{Ti}_{1-x})\text{O}_3$ thin films [16–18]. Additionally, the nature of the interaction of crystallographic defects with domains in low-ferroelastic-distortion systems remains an open question, and is also expected to vary with the scale of elastic energies particular to a given ferroelectric system.

$\text{SrBi}_2\text{Nb}_2\text{O}_9$ [as well as other isostructural $(\text{Ca}, \text{Sr}, \text{Ba})\text{Bi}_2(\text{Ta}, \text{Nb})_2\text{O}_9$ phases with very low ferroelastic distortion] serves as an end point in the spectrum

of ferroelectric materials, allowing experimental investigation of domain structure with a nearly zero contribution of elastic strain energy to the free energy balance controlling the structure. Prototypical perovskite ferroelectrics have a high ferroelastic distortion (e.g., 6.4% for PbTiO_3 [19]) and faceted 90° domains with high aspect ratios. The ferroelastic distortion of $\text{Bi}_4\text{Ti}_3\text{O}_{12}$, 0.82% [20] is 1 order of magnitude lower, and 90° domains [21] are faceted, but with a low aspect ratio [22]. The ferroelastic distortion of $\text{SrBi}_2\text{Nb}_2\text{O}_9$ is $<0.002\%$ [20], thus the elastic strain energy is several orders of magnitude smaller than for these other perovskite-based systems.

$\text{SrBi}_2\text{Nb}_2\text{O}_9$ is an Aurivillius phase [23,24] consisting of alternating layers of $\text{SrNb}_2\text{O}_7^{2-}$ perovskite and $\text{Bi}_2\text{O}_2^{2+}$. It belongs to the space group $A2_1am$, with lattice parameters $a = 5.5094(4)$ Å, $b = 5.5094(4)$ Å, and $c = 25.098(3)$ Å at room temperature [20]. Given this crystallographic setting, the existence of centric symmetry elements means that neither the b nor the c axis can support components of the spontaneous polarization; the spontaneous polarization lies entirely along the a axis of the orthorhombic cell [25]. Polar and nonpolar directions orthogonal to the c axis are distinguished solely on the basis of symmetry, with negligible accompanying distortion of the unit cell. Group theory has been used to deduce possible domain variants for this space group [5]; of particular interest are 90° rotation twins about c . In this work, the 90° ferroelectric domain structure of epitaxial $\text{SrBi}_2\text{Nb}_2\text{O}_9$ films is resolved by Bragg filtering of high-resolution transmission electron microscope (HRTEM) images.

Epitaxial (001) $\text{SrBi}_2\text{Nb}_2\text{O}_9$ films were grown on (001) SrTiO_3 by pulsed laser deposition as described elsewhere [26–28]. Great care was taken to avoid the introduction of sample artifacts by minimizing mechanical and thermal treatments during TEM sample preparation, and by minimizing beam exposure in the TEM during imaging. A JEOL 4000-EX II operated at 400 kV was used for high-resolution imaging at room temperature. HRTEM

phase contrast images were acquired using a 100 μm condenser aperture (convergence semiangle = 0.85 mrad), along separate, orthogonal zone axes: (1) along $[100]/[010]$, or $\langle 110 \rangle$ of the high-temperature tetragonal phase, in cross section, and (2) along $[001]$, in plan view. Standard bright-field TEM techniques typically employed to image ferroelectric domain structures rely on strain or δ -fringe-type contrast. However, these methods are exceedingly difficult to apply to this very-low ferroelastic distortion material because only a change in symmetry exists across a domain boundary. Instead, we rely on imaging using reflections unique to a given polar orientation.

A HRTEM image typically contains several spatial periodicities, roughly corresponding to the lattice planes from which diffracted beams arise. The Fourier transform (power spectrum) of a HRTEM image reveals these periodicities as spots, analogous to a diffraction pattern. It is possible to obtain a map of the regions of a HRTEM image containing specific spatial periodicities by selecting those frequencies in the Fourier transform with a mask, and performing a back transformation. Resolution of such maps is then limited by, and inversely proportional to, the aperture size of the mask. Conversely, signal-to-noise ratio is roughly proportional to the aperture size of the mask, such that an optimum aperture can be empirically determined for a given image.

4096×4096 pixel scans of real-space images were filtered with circular feathered masks in Fourier space to retain only intensity occurring at Bragg peaks unique to a specific ferroelectric domain type. These were 011 and 013 reflections with aperture radius $r = 0.4 \text{ nm}^{-1}$ for cross section samples, and 100 and 120 with $r = 0.2 \text{ nm}^{-1}$ for the plan-view samples. Peaks were selected from symmetry-allowed reflections [25] unique to one polar orientation; note, however, that the 100 results from double diffraction. This reflection has a high signal-to-noise ratio due to its low diffraction angle, and strong contrast transfer of the corresponding spatial periodicity at the chosen defocus. The reflection is unique to a specific domain type, and the spatial information it contains is considered significant due to the geometry of diffraction in the TEM. Note also that contrary to intuition, unique reflections in cross section arise from momentum transfer with no component along the polar axis. Masked regions were inverse transformed, and the amplitude components of the resulting complex images are presented here.

Figure 1 shows a representative $[100]/[010]$ phase-contrast TEM image obtained by cross section (a) and the corresponding ferroelectric domain map (b), generated using the 011 and 013 Bragg peaks. Bright regions are domains with spontaneous polarization perpendicular to the plane of the image. Dark regions are either domains with spontaneous polarization in the plane of the image, or are ferroelectrically inactive regions. Image features smaller than $\sim 1/r$ are attributable to the amorphous background.

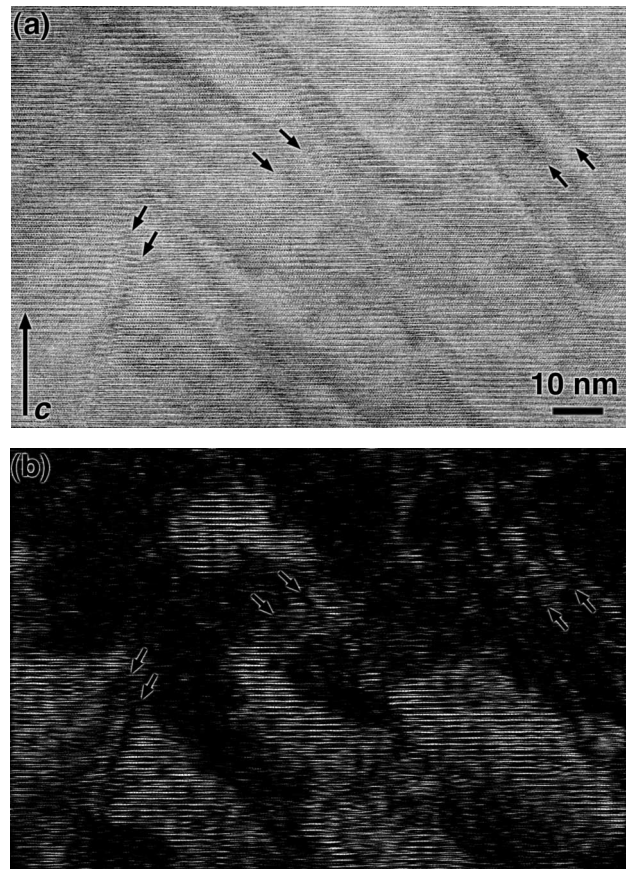


FIG. 1. A cross-sectional phase-contrast TEM image of a $\text{SrBi}_2\text{Nb}_2\text{O}_9$ epitaxial film along $[100]/[010]$. (Some regions are viewed along $[100]$, and others along $[010]$, due to the presence of ferroelectric domains. See Ref. [28].) (b) Bragg filtering to retain only the 011 and 013 periodicities reveals the 90° ferroelectric domain structure. Regions of bright contrast correspond to domains with the polarization axis perpendicular to the plane of the image. Dark areas are either regions polarized horizontally in the image plane, or are out-of-phase boundaries (examples arrowed).

The morphology of the 90° ferroelectric domain structure, as viewed along this axis, is controlled by essentially dipole-dipole effects and domain wall energy only. It is clear that the domain walls for this configuration are not faceted, but are instead highly irregular. This is in contrast to the morphology of 90° ferroelectric domains in high-distortion materials, which display a high aspect ratio with strongly crystallographically faceted domain walls [14,29,30]. 180° domain structures, on the other hand, do not have an associated strain energy component, and exhibit domain walls with a surface normal that meanders in the plane perpendicular to the spontaneous polarization [31], yielding morphologies similar to those imaged in $\text{SrBi}_2\text{Nb}_2\text{O}_9$ along this azimuth.

Dark bands (examples arrowed) in Fig. 1 correspond to out-of-phase boundaries (OPBs) [32]. Figure 2 shows a $[100]/[010]$ electron diffraction pattern of the same region shown in Fig. 1. The intensities of $h0l/0kl$ reflections corresponding to h or $k = 0$ or $2n$, and $l = 2n$, arise from all regions of the image. These spots are streaked in directions

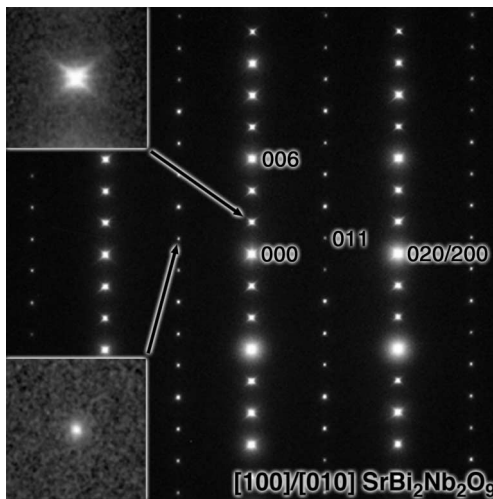


FIG. 2. Electron diffraction pattern taken along the $[100]/[010]$ $\text{SrBi}_2\text{Nb}_2\text{O}_9$ zone axis of the same film shown in Fig. 1. Reflections arising from both orientations are streaked 40° relative to $[001]^*$, and along $[100]^*$ or $[010]^*$, perpendicular to the habit planes of the defects. Reflections corresponding only to regions with polarization directions perpendicular to the image plane of Fig. 1 ($0kl, k, l = 2n - 1$) do not show streaking.

40° to $[001]^*$ and weakly along $[100]^*/[010]^*$, indicating habit planes of $\sim(014)/(104)$ and $(100)/(010)$ for the OPBs. Reflections with $h0l, h, l = 2n - 1$ are forbidden. $0kl, k, l = 2n - 1$ reflections arise only from regions of the specimen oriented with $[100]$ parallel to the electron beam; these reflections do not display streaking. Selected-area Fourier analysis of the real space image, along with the fact that OPBs are dark in the domain image, indicate the OPBs do not contribute to these nonstreaked reflections. Therefore, it is likely that, at least along this azimuth, OPBs display a higher symmetry than the bulk crystal (as evidenced by more systematic absences, indexed using the unfaulted crystal's reciprocal lattice), and may not reflect the polarity of bulk $\text{SrBi}_2\text{Nb}_2\text{O}_9$. Figure 3 shows a low-magnification image of the same film shown in Figs. 1 and 2. A ferroelectric domain map of the type shown in Fig. 1(b) is overlaid on the region of the image from which it was derived. This figure demonstrates the lack of preferred orientation for 90° ferroelectric domain walls on a greater length scale, and also shows the weak spatial correlation of domain walls and OPBs, which may be due to OPBs acting as nucleation sites for ferroelectric domains.

A high-resolution TEM image of a $\text{SrBi}_2\text{Nb}_2\text{O}_9$ film, viewed in plan-view along $[001]$, was Bragg filtered to reveal the two 90° ferroelectric domain types, shown in Figs. 4(a) and 4(b). Bright regions are ferroelectric domains with their polar axes as indicated in the figures. Contrast in this azimuth is reduced (1) because of the highly irregular domain structure projected along this viewing axis, which corresponds to the film thickness (c -) direction of Figs. 1 and 3, and (2) because the $hk0$ reflections used for imaging are quite weak in comparison

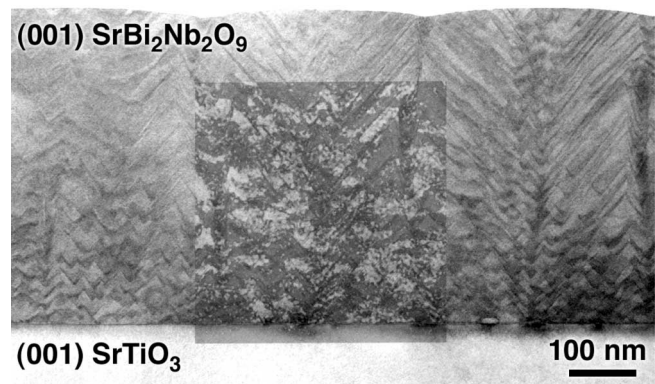


FIG. 3. TEM image along $[100]/[010]$ of the same film shown in Figs. 1 and 2. A Bragg-filtered image of the center region is overlaid on the image, showing the ferroelectric domain structure on a large scale, and also showing the weak correlation between 90° ferroelectric domain walls and the out-of-phase boundaries, which are visible as diagonal bands of contrast in the image.

to those used for imaging along the previously described azimuth. Comparison of Figs. 4(a) and 4(b) reveals that the domains are almost entirely complementary. Thus, this method successfully distinguishes the two domain variants, despite the poor contrast. Again, domain walls are not constrained to specific crystallographic orientations and appear to be highly curved.

The morphology of the 90° ferroelectric domain structure, as viewed along this axis, is controlled by electrostatic energy, as well as by dipole-dipole interactions and domain wall energy. For this orientation, 90° ferroelectric domain walls of any orientation other than 45° with respect to the polar axis have an associated space charge due to divergence in the component of the polarization normal to the domain wall. The fact that walls are so curved in this section therefore implies that $\text{SrBi}_2\text{Nb}_2\text{O}_9$ is fairly tolerant of such space charge.

In conclusion, the 90° ferroelectric domain structure of $\text{SrBi}_2\text{Nb}_2\text{O}_9$ has been resolved. Out-of-phase boundary (OPB) defects are shown to be weakly correlated with the domain morphology. Ferroelectric domain walls are

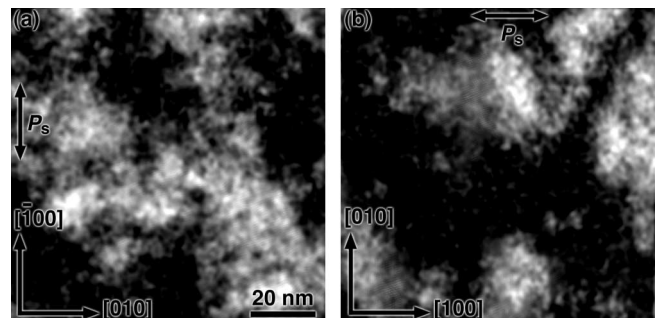


FIG. 4. Ferroelectric domains in a $\text{SrBi}_2\text{Nb}_2\text{O}_9$ epitaxial film, viewed along $[001]$. Bragg filtering of a phase contrast image to retain only the 100 and 120 periodicities reveals the two 90° ferroelectric domain types, (a) and (b). Regions of bright contrast correspond to domains with the spontaneous polarization oriented as indicated in the images.

highly curved both in the a - b plane, and perpendicular to that plane. The vanishingly small ferroelastic distortion of $\text{SrBi}_2\text{Nb}_2\text{O}_9$ has enabled experimental observation of a ferroelectric domain structure that is determined by dipole-dipole interaction and domain wall energies, both with and without an electrostatic energy contribution, and with a negligible contribution from strain energy. These results provide experimental separation of the effects of the energetic contributions dictating ferroelectric domain structure. An as-yet unaddressed technological benefit of this low ferroelastic distortion is that mechanically constrained devices fabricated from these materials are expected to be less susceptible to strain-induced polarization clamping. These results also demonstrate that the highly faceted nature of typical ferroelectric domain structures is primarily a result of strain energy.

The authors gratefully acknowledge the financial support of the National Science Foundation through Grant No. DMR-0103354 and, for the work performed at ANL, the U.S. Department of Energy through Contract No. W-31-109-ENG-38. TEM analysis was performed at the Electron Microscopy Collaborative Research Center at Argonne National Laboratory. The authors also thank Michael O'Keefe and Karl Merkle for helpful discussions.

*Corresponding author.

Electronic address: maz132@psu.edu

- [1] J. Fousek and V. Janovec, *J. Appl. Phys.* **40**, 135 (1969).
 [2] F. Tsai, V. Khiznichenko, and J.M. Cowley, *Ultramicroscopy* **45**, 55 (1992).
 [3] S. K. Streiffer *et al.*, *J. Appl. Phys.* **83**, 2742 (1998).
 [4] A. L. Roytburd *et al.*, *J. Appl. Phys.* **89**, 553 (2001).
 [5] Y. Ding, J. S. Liu, and Y. N. Wang, *Appl. Phys. Lett.* **76**, 103 (2000).
 [6] A. Gruverman *et al.*, *Appl. Phys. Lett.* **76**, 106 (2000).
 [7] Y. Ding, J. S. Liu, I. MacLaren, and Y. N. Wang, *Appl. Phys. Lett.* **79**, 1015 (2001).
 [8] X. Zhu *et al.*, *Appl. Phys. Lett.* **78**, 799 (2001).
 [9] S. Nambu and D. A. Sagala, *Phys. Rev. B* **50**, 5838 (1994).
 [10] H. L. Hu and L. Q. Chen, *J. Am. Ceram. Soc.* **81**, 492 (1998).
 [11] S. Semenovskaya and A. G. Khachatryan, *J. Appl. Phys.* **83**, 5125 (1998).
 [12] B. G. Potter, Jr., V. Tikare, and B. A. Tuttle, *J. Appl. Phys.* **87**, 4415 (2000).
 [13] F. Jona and G. Shirane, *Ferroelectric Crystals*, International Series of Monographs on Solid State Physics Vol. I (Pergamon, Oxford, 1962), p. 162.
 [14] M. Tanaka and G. Honjo, *J. Phys. Soc. Jpn.* **19**, 954 (1964).
 [15] J. F. Scott, *Ferroelectrics Rev.* **1**, 1 (1998).
 [16] M. O. Eatough *et al.*, in *Ferroelectric Thin Films IV*, edited by B. A. Tuttle, S. B. Desu, R. Ramesh, and T. Shiosaki (Materials Research Society, Warrendale, PA, 1995), p. 111.
 [17] S. Trolier-McKinstry *et al.*, *Ferroelectrics* **206**, 381 (1998).
 [18] A. L. Kholkin *et al.*, *J. Appl. Phys.* **89**, 8066 (2001).
 [19] *Landolt-Börnstein: Numerical Data and Functional Relationships in Science and Technology*, edited by K.-H. Hellwege and A. M. Hellwege (Springer-Verlag, Berlin, 1981), New Series, Group III, Vol. 16, Part a, p. 360.
 [20] A. D. Rae, J. G. Thompson, R. L. Withers, and A. C. Willis, *Acta Crystallogr. Sect. B* **46**, 474 (1990).
 [21] Polarization lies almost entirely along a^* (8% along c). S. E. Cummins and L. E. Cross, *J. Appl. Phys.* **39**, 2268 (1968).
 [22] Y. Barad, J. Lettieri, C. D. Theis, D. G. Schlom, J. C. Jiang, and X. Q. Pan, *J. Appl. Phys.* **89**, 1387 (2001).
 [23] B. Aurivillius, *Ark. Kemi* **1**, 463 (1950); **1**, 499 (1950); **2**, 519 (1951); **5**, 39 (1953).
 [24] B. Aurivillius and P. H. Fang, *Phys. Rev.* **126**, 893 (1962).
 [25] *International Tables for Crystallography, Volume A: Space-Group Symmetry*, edited by T. Hahn (Kluwer Academic Publishers, Dordrecht, 1996), 3rd ed., p. 788; *ibid.*, p. 230.
 [26] J. Lettieri *et al.*, *Appl. Phys. Lett.* **73**, 2923 (1998).
 [27] J. Lettieri *et al.*, *Thin Solid Films* **379**, 64 (2000).
 [28] At growth temperature the (001) $\text{SrBi}_2\text{Nb}_2\text{O}_9$ epitaxial film is tetragonal and grows with a single orientation relationship. On cooling through the Curie temperature, however, the a and b axes of $\text{SrBi}_2\text{Nb}_2\text{O}_9$ become distinct and the film twins into ferroelectric domains in which either the a or the b axis of $\text{SrBi}_2\text{Nb}_2\text{O}_9$ lies parallel to [110] SrTiO_3 .
 [29] E. K. Goo, R. K. Mishra, and G. Thomas, *J. Appl. Phys.* **52**, 2940 (1981).
 [30] C. A. Randall, D. J. Barber, and R. W. Whatmore, *J. Mater. Sci.* **22**, 825 (1987).
 [31] G. L. Pearson and W. L. Feldman, *J. Phys. Chem. Solids* **9**, 28 (1959).
 [32] M. A. Zurbuchen *et al.*, *J. Mater. Res.* **16**, 489 (2001).